Mon. Not. R. astr. Soc. (1986) **219**, 791–808

A dynamical model for the dwarf nova AH Herculis[1]

Keith Horne *Institute of Astronomy, Madingley Road, Cambridge CB3 0HA and Space Telescope Science Institute, Homewood Campus, Baltimore, MD 21218, USA*

Richard A. Wade *Steward Observatory, University of Arizona, AZ 85721, USA*

Paula Szkody *Department of Astronomy, University of Washington, Seattle, WA 98195, USA*

Accepted 1985 October 30. Received 1985 October 30; in original form 1985 August 16

Summary. We develop a dynamical model of the dwarf nova binary AH Herculis based upon high-resolution phase-resolved spectroscopy from the 2.5-m Hooker reflector at Mt Wilson. The distorted double-peaked Balmer emission lines from the accretion disc surrounding the white dwarf primary star have a peak-to-peak separation of 600 km s^{-1}. From radial velocity variations of the emission lines over a one-year baseline we determine the binary period $P=0.258116\pm0.000004$ day. We detect the weak absorption spectrum of the cool mass-losing companion star AH Her B, and use a cross-correlation method to measure its orbit radial velocity curve. The spectral type of AH Her B is early-to-middle K, but the Mg b lines are much weaker than expected relative to Fe I. The radial velocity semi-amplitudes $K_{\mathrm{ems}}=126\pm4$ km s^{-1} for the emission line wings and $K_{\mathrm{abs}}=158\pm8$ km s^{-1} for the absorption lines imply mass functions $M_W \sin^3 i=0.34\pm0.04\,M_\odot$, $M_R \sin^3 i=0.27\pm0.03\,M_\odot$, and $a \sin i=1.45\pm0.05\,R_\odot$. If we impose an empirical ZAMS mass–radius relationship on the companion star, then $i=46°\pm3°$, $M_W=0.95\pm0.10\,M_\odot$ and $M_R=0.76\pm0.08\,M_\odot$.

1 Introduction

Cataclysmic variables are close binary star systems in which a white dwarf star accretes matter lost through Roche-lobe overflow from its cool dwarf companion star. Photometric and spectroscopic variations have revealed many accurate binary periods for these systems, but the determination of other dynamical parameters has proven to be a more difficult challenge. The white dwarf's orbital motion must usually be inferred from measurements of broad emission lines that arise in the surrounding accretion disc. Strong continuum radiation from the disc diminishes the equivalent widths of absorption lines from the cool star, often making them undetectable with the

[1] Based on observations carried out at Mt Wilson Observatory, Carnegie Institution of Washington.

short exposure times that are required to resolve the binary motion. The use of linear detectors now provides digital data that can be manipulated in ways that in large measure overcome these problems.

AH Herculis is a dwarf nova of the Z Cam class that varies from $V{\sim}14.3$ in quiescence to $V{\sim}11.3$ during outbursts that last 4–18 day and recur at intervals of 7–27 day (Szkody & Mattei 1984). A binary period of 0.247 ± 0.008 day was determined from photometric observations of AH Her during an 11 day interval covering the decline from an outburst in 1983 June (Moffatt & Shara 1984). This rather long binary period and a rising energy distribution in the near-infrared (Wade 1982), both suggest that absorption lines from the cool star should be easily detectable, yet they are not readily visible (Robinson 1973).

In this paper we develop a model for the AH Her binary based on the spectroscopic observations presented in Section 2. We find emission line radial velocity variations that confirm the photometric period and allow us to determine an accurate spectroscopic ephemeris (Section 3). By folding data on the spectroscopic period, we examine fine structure in the emission line profiles and derive a radial velocity curve from the emission line wings that are thought to reflect the orbital motion of the white dwarf primary (Section 4). We detect the weak absorption spectrum of the companion star (AH Her B) and use a cross-correlation analysis to measure its rotation and orbital motion (Section 5). Lastly, we examine a dynamical model for the AH Her system (Section 6).

2 Observations

We observed AH Her in moderate seeing with the Varo-Reticon detector and Coude spectrograph of the Mt Wilson 2.5-m telescope on five nights in 1980 June and on five nights during 1981 April, May, and June. We made short (600 or 900s) exposures of AH Her in sequences that lasted usually between three and six hours on each night. The 1980 observations covered a roughly 600 Å spectral range around Hβ; those in 1981 covered a similar range centred at Hα. The Varo image tubes caused the dispersion to vary from 0.15 at the ends to 0.25 Å/pixel near the centre of the 3744 pixel Reticon detectors. The spectral resolution (FWHM) was 5 to 6 pixels. Visual observations made by members of the AAVSO indicate that AH Her was near minimum in its outburst cycle during our observations. The visual magnitude estimates and additional details of our observations are collected in Table 1.

Table 1. Spectroscopic observations of AH Her.

Date (UTC)			HJD	Binary Phase		Spectra		λ	AAVSO	EW
	beg	end	beg	beg	end	No	dwell	(Å)	V(mag)	(Å)
1980			2444000+				(s)			Hβ
Jun	3.21	3.46	393.71	-0.46	0.50	19	900	4720-5270	13.9 Q	16.9
Jun	4.19	4.46	394.69	3.33	4.37	24	900	4720-5270	13.9 Q	10.5
Jun	5.18	5.37	395.68	7.19	7.91	17	900	4720-5270	13.4 R	8.0
Jun	16.24	16.40	406.74	50.03	50.63	10	900	4400-5000	13.7 D	5.4
Jun	19.19	19.43	409.69	61.46	62.35	21	900	4400-5000	14.3 Q	19.0
1981										Hα
Apr	5.35	5.50	699.85	1185.57	1186.28	22	600	6280-6780	13.0 D	13.2
May	9.25	9.49	733.75	1316.91	1317.83	21	900	6200-6780	14.3 Q	20.8
Jun	3.20	3.33	758.70	1413.58	1414.07	15	600	6280-6860	14.3 Q	14.4
Jun	5.27	5.32	760.77	1421.59	1421.85	8	600	6300-6850	14.3 Q	15.0
Jun	6.26	6.29	761.77	1425.45	1425.54	4	600	6300-6850	14.3 Q	16.7

Notes: Q=quiescence, R=rising, D=decline

The photon-counting Varo-Reticon is a low-noise, linear detector providing simultaneous measurements of sky and object spectra. After a 600 s exposure, the two arrays typically had recorded 50 000 photons from AH Her through a 1×3 arcsec^2 aperture and 6000 photons from a nearby equal-sized patch of blank sky. Observations of the twilight sky were used to calibrate the relative response of the two arrays, permitting accurate subtraction of the night sky spectrum from each object spectrum. The sensitivity along each array was calibrated on scales shorter than a few hundred pixels by long exposures to diffused light from a trungsten lamp, and on longer scales by observations of spectrophotometric standard stars.

A high signal-to-noise spectrum of argon was obtained for each night either from a long exposure made during the following morning or by summing the short argon exposures taken during the night. The positions of typically 22 argon lines were measured and fitted by a sixth order polynomial with a mean error of 0.05 Å. Quadratic corrections were applied to this primary wavelength calibration on the basis of measurements of six strong lines in short argon exposures that were interspersed with the observations of AH Her. The resulting corrections were small (<1 Å), and varied smoothly with the hour angle of AH Her.

3 The binary period and a preliminary ephemeris

Wargau, Rahe & Vogt (1983) have suggested that the binary period of AH Her is $P=5.9\pm0.5$ hr, based on measurements of the rate of decline after outbursts and broadband colours in quiescence. Echevarria (1983) made a similar prediction based on broadband photometry (Echevarria & Jones 1984). Indeed, our original choice of AH Her as a system for study was motivated by the similarity of its spectral energy distribution in quiescence to that of SS Cyg, based on the data later published in Oke & Wade (1982).

Extensive photometric observations of AH Her during quiescence have yielded no evidence for the binary period (Bretz 1965; Stiening, private communication). The system is also well observed during outbursts to study the rapid oscillation which appears at periods of 24–39 s at these times (Hildebrand *et al.* 1980; Hildebrand, Spillar & Stiening 1981; Patterson 1981). No reports of systematic photometric variation indicating the binary period emerged from these studies until the observations of Moffatt & Shara (1984) indicated a period of 0.247 ± 0.008 day.

To search for spectroscopic evidence of the binary period, we measured a radial velocity for the Balmer emission line in each of our 161 spectra. A polynomial fit was used to flatten the continuum, and velocities were measured by fitting a Gaussian line profile (FWHM=1000 km s^{-1}) to the data by the method of weighted least squares. The fixed dispersion of the Gaussian was chosen to match the emission line profile in the grand average of all the AH Her spectra.

Plots of the emission line radial velocity as a function of time on individual nights revealed variations indicating a period of about 6 hr. We searched for the best-fitting period in a wide range of periods about 6 hr. For each trial period P we fitted a circular orbit

$$V(t)=\gamma+K\sin\frac{2\pi(t-t_0)}{P} \qquad (1)$$

to several subsets of the emission velocity measurements by adjusting the orbit parameters γ, K, and t_0.

We first consider the data from 1980 June 3–5, which provide the best discrimination against aliases of 1 cycle/day. Fig. 1(a) shows the behaviour of χ^2, the normalized weighted sum of squared residuals to the fit, as a function of trial period P for this subset of the data. A series of narrow dips, separation by 1 cycle/day, defines an envelope whose breadth is determined by the

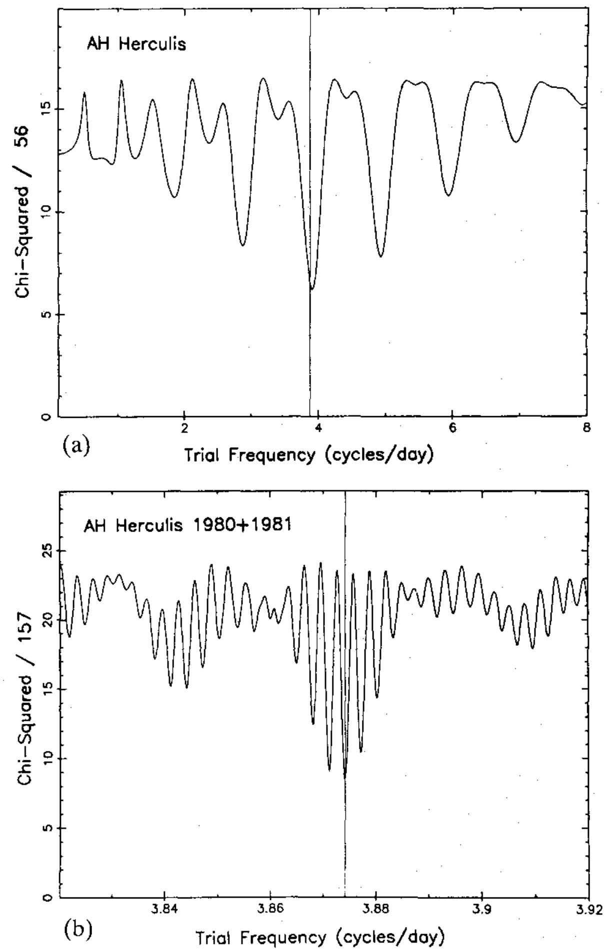

Figure 1. The χ^2 achieved by a sinusoid fit to emission line radial velocity measurements is shown as a function of the assumed orbit frequency. The frequency structure obtained from 1980 June 3–5, showing the 1 cycle/day aliases, is given in 1(a) while that for the entire data set, spanning a year, is given in 1(b). The adopted period is indicated by a vertical line.

duration of the observations on the individual nights. The most likely period, near 0.258 day, is consistent with the photometric period of 0.247±0.008 day found by Moffatt & Shara (1984). (The reduced χ^2 for this best-fitting period exceeds the expected value of unity because intrinsic variations in the profile of the emission line introduce velocity errors that are larger than the velocity uncertainty computed from photon statistics.)

We focus further attention on periods near 0.258 day. The 1980 Hβ and 1981 Hα data sets, providing time bases of 60 and 240 binary cycles, supply the period estimates 0.2586±0.0003 and 0.2581±0.0001 day. The 1980 and 1981 data sets may be combined, assuming that the Hβ and Hα lines follow the same radial velocity curve, to yield a time base of about 1400 cycles. For this complete radial velocity data set, the behaviour of χ^2 as a function of trial period is shown in Fig. 1(b). Two periods, differing by 1 cycle/yr, appear to be possible. We adopt the most probable period, 0.25812±0.00001 day, as the best estimate of the binary period of AH Her. Fig. 2 displays the emission velocities folded on this period. The rms scatter of the measured velocities about the fitted sine curve is 44 km s^{-1}. No evidence was found for deviation from a constant period, but the upper limit on $\dot{P}$ is only 10^{-4} s s^{-1}.

Binary phases used throughout this paper are computed with respect to the preliminary

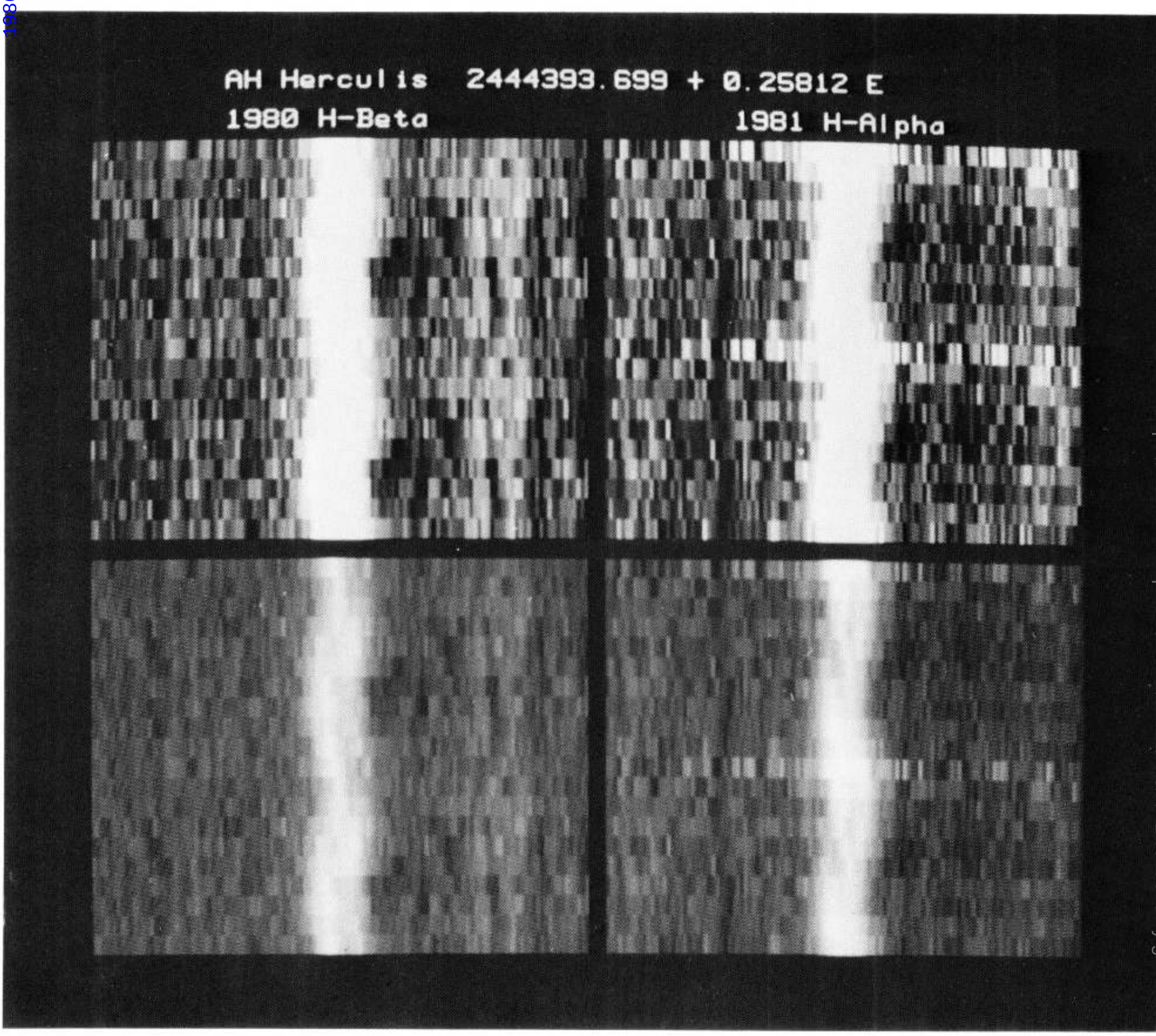

Plate 1. Trailed-spectrogram representations of the orbital variations at Hα and Hβ. The data were averaged into 10 equal phase bins, and are displayed through two full orbit cycles beginning with $\phi=0$ at the bottom of each panel. Two versions of the spectrogram are shown for each wavelength region, to bring out structure near the peaks of the lines and near the continua.

[*facing page* 794]

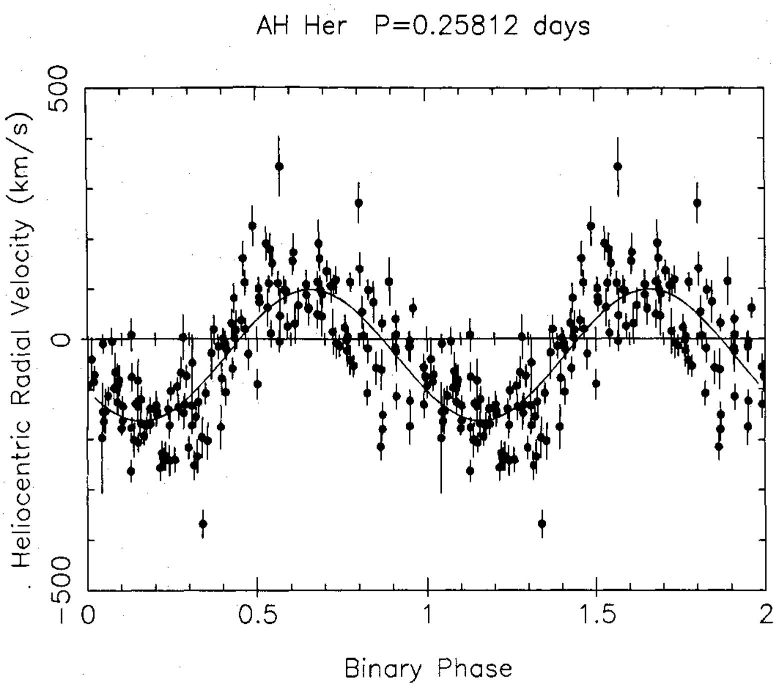

Figure 2. The emission line radial velocities are folded on the best-fit binary period.

spectroscopic ephemeris

$$HJD = 2\,444\,393.699 + 0.25812\,E. \quad (2)$$

The epoch chosen here corresponds approximately to superior conjunction of the white dwarf. A slightly revised final ephemeris, based on measurements in the emission line wings and of absorption lines from the secondary star, is given in Section 5.3.

4 Analysis of the emission lines

4.1 EMISSION LINE PROFILES

Variations in the nightly mean equivalent width of the Hα and Hβ emission lines are noted in Table 1. We also witnessed erratic variations in the equivalent widths by factors of up to 2 on time-scales comparable to the 600 or 900 s exposure times. Such variations may be associated with rapid variations in the continuum of AH Her, a phenomenon widely known as 'flickering' from high-speed photometric studies of cataclysmic variables. We folded the equivalent widths on the binary period to search for systematic variations in the line strengths, but no strong trends were apparent.

To reduce noise and bring out weak features in the data, we based further measurements of AH Her on spectra averaged in 10 phase bins equally spaced around the binary orbit. Plate 1 exhibits the phase-binned Hα and Hβ line profiles in the form of trailed spectrograms. Two panels are given for each line, one emphasizing the wings of the line profile and the other the peaks. The sequence of 10 spectra is duplicated to simulate the appearance of two full binary cycles; the bottom, middle and top of each panel correspond to phase 0 on successive cycles. The continua are normalized to a common grey level. The number of individual spectra involved in each bin average ranges from 2–12, and the noise level accordingly varies from bin to bin.

Orbital variations in the emission line velocity are clearly visible in Plate 1. An absorption line from AH Her B is visible to the left of Hα. The lower panels of Plate 1 indicate that similar structure is present in both the Hα and Hβ line profiles, which were measured in different years. A double-peaked morphology with a peak-to-peak separation of $600\pm980\,\mathrm{km\,s^{-1}}$ is present at most phases, but the line profiles are more complex than model line profiles for simple Keplerian discs (Smak 1969). The Hβ emission is systematically stronger on the blue side of its profile. Both lines show a sharp emission component that emerges from the red peak around phase 0.3–0.4, crosses the centre of the line profile around phase 0.5, and merges with the blue peak around phase 0.7–0.8. The phasing suggests that this component is associated with the stream of gas from the companion star or with disturbances produced by it in the outer parts of the accretion disc. The sharp component might also represent chromospheric emission on the side of the companion star illuminated by the disc.

Fig. 3 shows mean line profiles obtained by averaging the 10 phase-binned spectra after removal of the orbital motion of the emission line wings (Section 4.2). The mean profiles of both Hα and Hβ are double-peaked, although the cusps are not as pronounced as is expected from simple models of emission from Keplerian accretion discs (Smak 1969). The blue peak of Hβ is stronger in the mean than the red peak. The $600\pm80\,\mathrm{km\,s^{-1}}$ peak-to-peak separation may be interpreted as the projected Keplerian velocity at the outer rim of the disc. Emission is detected on either side of line centre to at least $1100\,\mathrm{km\,s^{-1}}$ for Hβ and to $1300\,\mathrm{km\,s^{-1}}$ for Hα.

Figs 4 and 5 display spectra covering a wider wavelength range (discussed further in Section 5.1). The uppermost spectrum in each figure is an average of the individual spectra, after each has been corrected to the velocity frame of the white dwarf. The broad Balmer emission lines are the strongest features in the spectra; we tabulate their mean equivalent widths on each night in Table 1. We attribute similarly broad but much weaker emission occurring near $\lambda\lambda$4920, 5015, 5165, and 6680 to He I lines at $\lambda\lambda$4921, 5015, and 6678 and with multiplet 42 of Fe I at $\lambda\lambda$4924, 5018, and 5169.

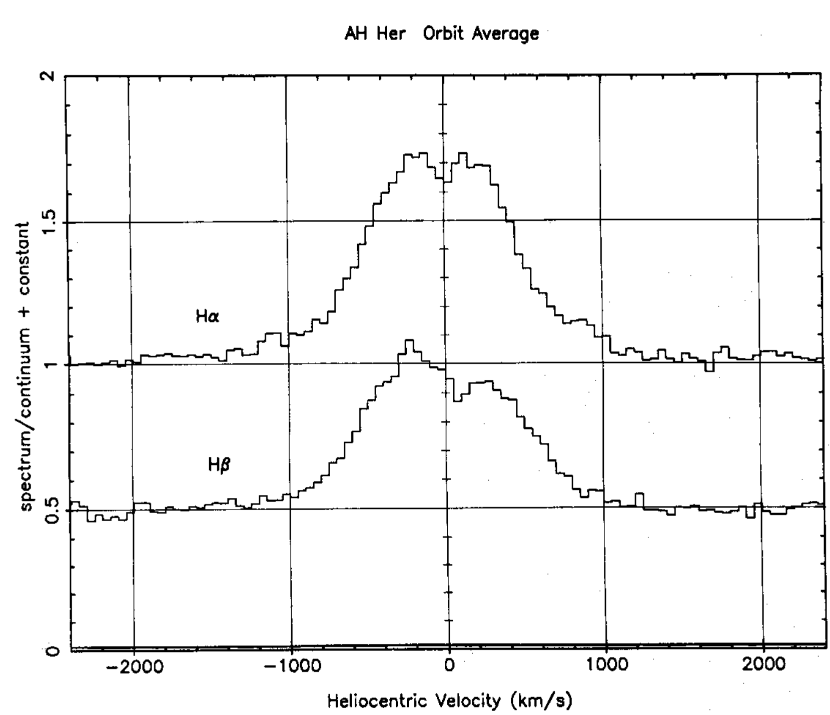

Figure 3. The mean profiles of Hα and Hβ obtained by averaging the 10 phase-binned spectra, after shifting each to correct for the motion of the white dwarf. The data are shown on a velocity scale.

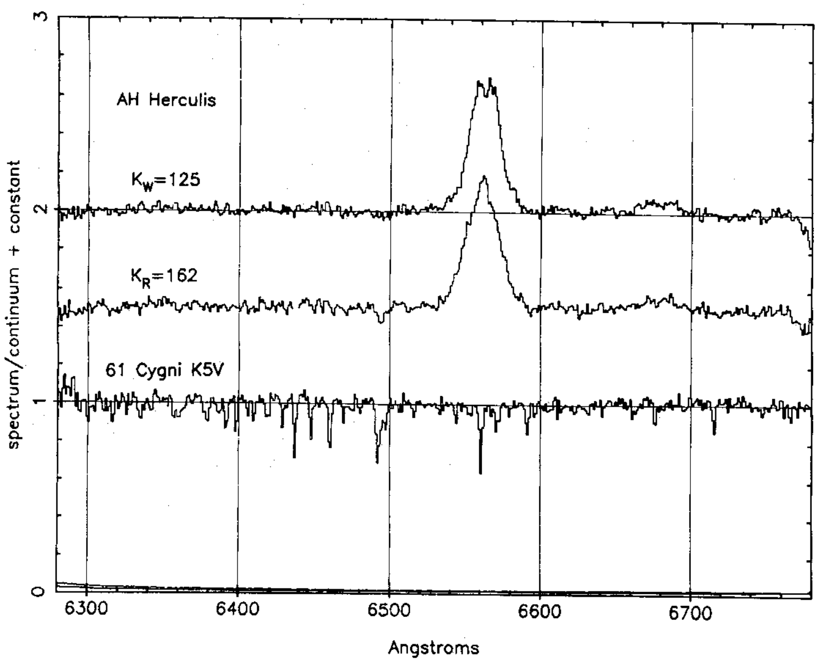

Figure 4. Top: 'Phased' spectrum of AH Her in the region around Hα. Seventy-one spectra of AH Her comprising a total exposure of 13.4 hr were averaged together after velocity shifts were applied to remove the orbital variation of the emission lines. Middle: Phased spectrum of AH Her in which the orbital motion of the absorption lines has been removed. Bottom: The spectrum of 61 Cyg A.

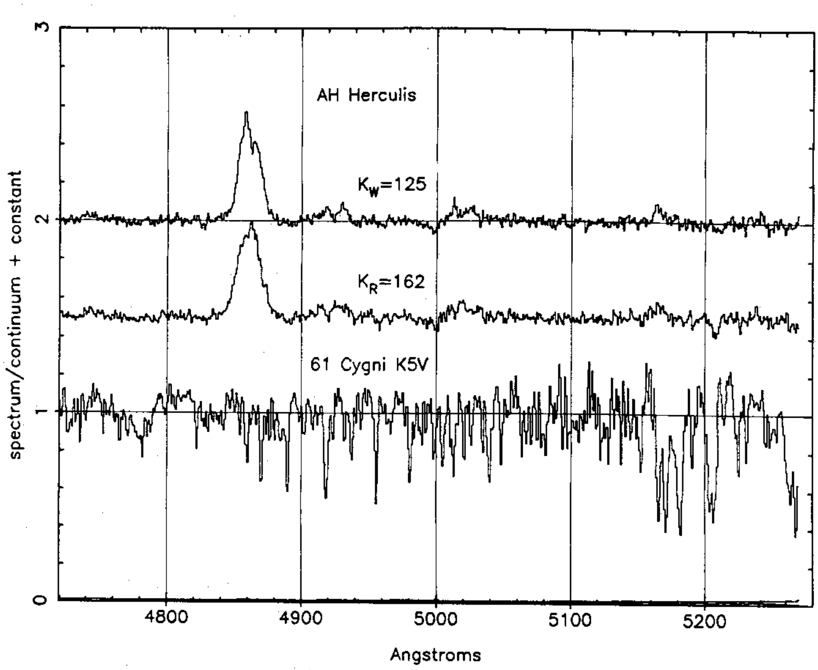

Figure 5. Same as Fig. 4, for the spectral region around Hβ. The total exposure on AH Her is 14.8 hr.

4.2 VELOCITIES FROM THE EMISSION LINE WINGS

Motivation for using the line profile wings to determine radial velocities is provided by an expectation that the wings form in a region close to the white dwarf, where disruption of the expected symmetry about the white dwarf by the influence of the companion star and gas stream should be small. Radial velocities measured from the wings are more sensitive to statistical noise, but should trace the orbital motion of the white dwarf more faithfully than the 'bulk' velocities that we measured to determine the binary period.

We measured velocities for the wings of the Balmer emission lines with the algorithm originally developed by Schneider & Young (1980) and adopted by Shafter (1983). The algorithm finds the velocity that maximizes the cross-correlation between the digital spectrum and an analytic template line profile. The line velocity V is found by a Newton–Raphson iterative solution of the equation

$$0=\sum_i D_i G'(v_i-V), \tag{3}$$

where D_i is the spectrum data at wavelength λ_i, $v_i=c(\lambda_i-\lambda_0)/\lambda_0$ is the corresponding velocity, and $G'(v)$ is the derivative of the template velocity profile $G(v)$. Assuming that the data D_i are statistically independent, the variance of the velocity estimate V is given by

$$\mathrm{var}(V)=\frac{\sum_i \mathrm{var}(D_i)\{G'(v_i-V)\}^2}{\left|\sum_i D_i G''(v_i-V)\right|^2}, \tag{4}$$

where $\mathrm{var}(D_i)$ denotes the variance of D_i, and $G''(v)$ is the second derivative of the template velocity profile. Poisson (photon-counting) statistics provided estimates for $\mathrm{var}(D_i)$.

The algorithm offers the freedom to choose the model profile $G(v)$. To measure a velocity for the wings of an emission line, a flat-topped template profile is constructed such that its derivative $G'(v)$ is the difference of two equal Gaussians that are separated by a chosen velocity interval S:

$$G'(v)=\exp\left\{-\frac{(v-S/2)^2}{2\sigma^2}\right\}-\exp\left\{-\frac{(v+S/2)^2}{2\sigma^2}\right\}. \tag{5}$$

With this choice the algorithm in effect compares the emission line flux in two Gaussian bandpasses displaced by $\pm S/2$ to either side of line centre, and finds the velocity of line centre for which the two fluxes are equal. By choosing suitable values for the Gaussian dispersion σ and the separation S between the Gaussians, we can study the velocity behaviour of specific parts of the line profile.

We measured wing velocities for the emission lines of AH Her by using twin Gaussians ($200\,\mathrm{km\,s^{-1}}$ FWHM), as described above. Fig. 6 shows the wing velocities and their fitted sine curves for separations S ranging from 600 to $2000\,\mathrm{km\,s^{-1}}$. Results obtained with a single Gaussian of $1000\,\mathrm{km\,s^{-1}}$ FWHM (as used in Section 3 above) are also shown. Fig. 7 shows the dependence of the fitted orbit parameters K, γ, and ϕ_0 on the Gaussian separation S. The fiducial phase ϕ_0 is the phase at which the velocity of the line crosses the γ velocity from blue to red; for the white dwarf this is expected to occur at phase 0.5.

Figs 6 and 7 show that the velocity curve for $S<1000\,\mathrm{km\,s^{-1}}$ departs from the expected orbit of the white dwarf; the shape of the velocity curve is not sinusoidal, Hα and Hβ have different γ velocities, and the fiducial phase ϕ_0 is less than 0.5. These systematic errors decrease as higher velocities in the wings are sampled; the velocity curve becomes consistent with a sine curve, the fiducial phase increases until it is stable and consistent with $\phi_0=0.5$, and the γ velocities of Hα and Hβ agree. At the same time, however, statistical uncertainties grow as S increases and the emission flux in the line wings eventually becomes smaller than the noise due to the continuum. Thus to determine the orbit of the white dwarf it is desirable to measure emission line velocities as far into the wings as possible, but not so far as to degrade the statistical accuracy of the velocities.

We therefore adopted weighted averages of $K_{\rm ems}$, γ and ϕ_0 from the measurements at 1200, 1400, 1600 and 1800 km s^{-1} separation to represent the motion of the white dwarf. The resulting orbit parameters are given in Table 2. The wings of Hα and Hβ give consistent orbit parameters. We adopt $K_{\rm ems}$=126±4 km s^{-1} as the best estimate of the white dwarf K velocity.

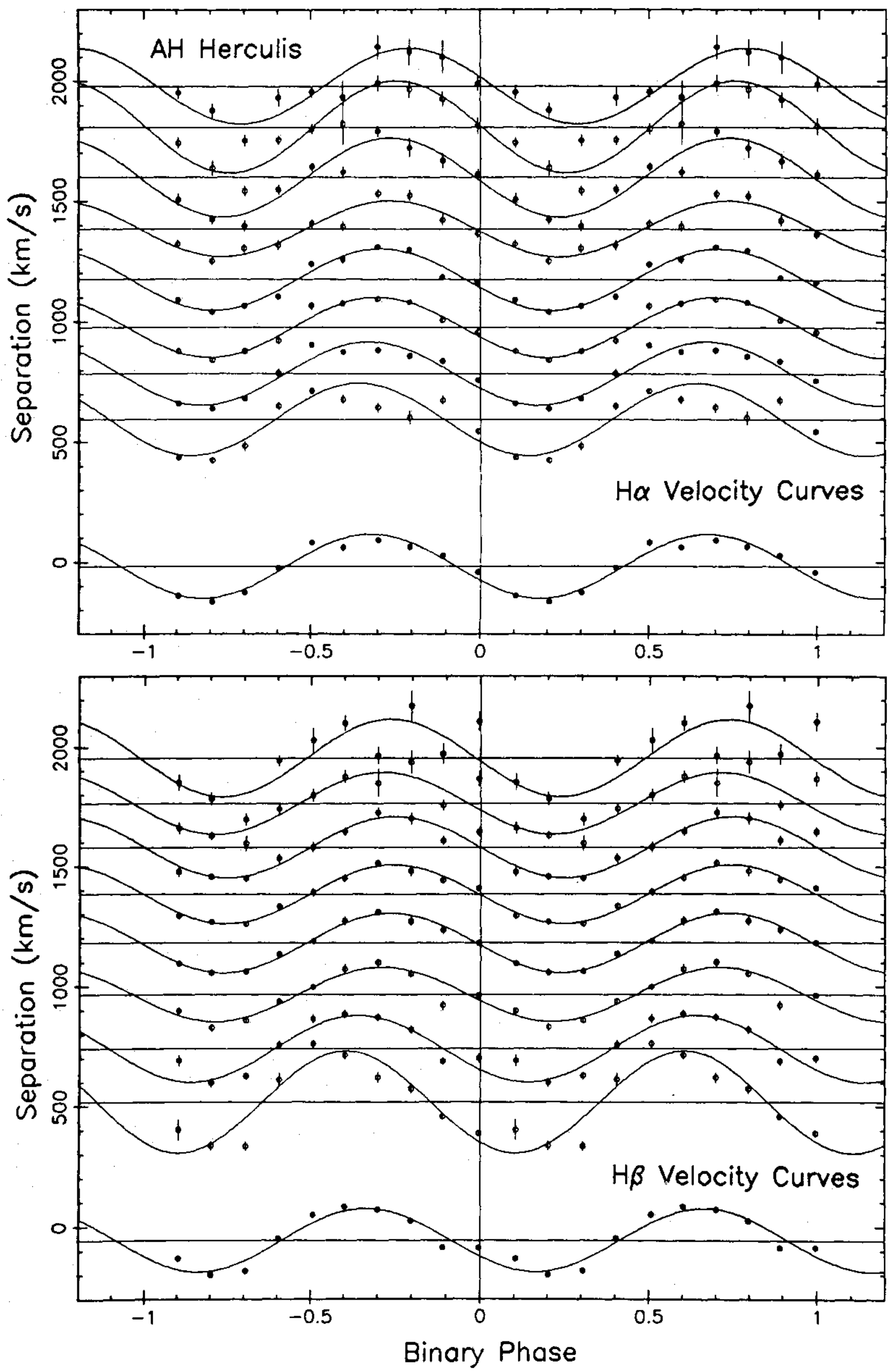

Figure 6. The measured velocity curves and their best-fit sinusoids for a range of positions in the wings of the emission lines. The velocities were measured by comparing the emission flux in two Gaussian bandpasses separated by a fixed velocity interval S, as described in Section 4.2. Velocity curves are shown for S ranging from 600–2000 km s^{-1} in steps of 200 km s^{-1}. For separations smaller than 1000 km s^{-1}, the velocity curve is distinctly non-sinusoidal, and suffers an anomalous phase shift. Farther out into the wings the measured velocities become increasingly uncertain as continuum noise begins to take effect. Also shown, at the bottom in each panel, is the velocity curve obtained with the single-Gaussian fitting function of Section 3.

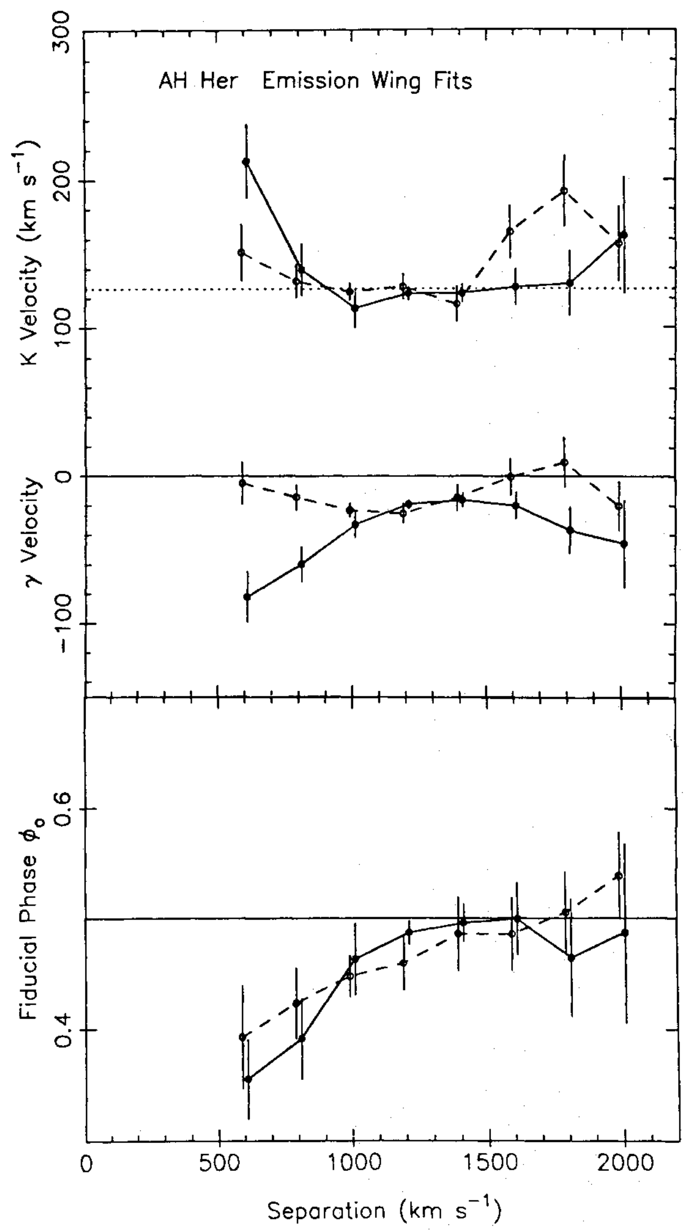

Figure 7. The orbit parameters K, γ and ϕ_0 fitted to the velocity curves of Fig. 6, are examined as a function of S, the separation into the emission line wings. Hα and Hβ results are indicated by open and filled symbols respectively. For $S<1000\,\mathrm{km\,s^{-1}}$, the H$\alpha$ and Hβ velocity curves have different γ velocities, and the fiducial phase ϕ_0 is less than that expected for the white dwarf orbit. These systematic errors decrease farther into the wings, but statistical uncertainties become larger. The adopted white dwarf K velocity, indicated by a dotted line, is a weighted average over separations larger than $1000\,\mathrm{km\,s^{-1}}$.

5 The secondary star

5.1 DETECTION AND ORBITAL MOTION OF AH Her B

We found no evidence for absorption lines by inspecting the individual spectra of AH Her. Robinson (1973) also failed to detect features on red image tube spectra. Our phase-binned spectra, shown in Plate 1 as a trailed spectrogram, reveal an absorption line near λ6495 that is moving in anti-phase with the Hα emission line. We attribute this feature, a blend of Ca I and Fe I lines which is strong in the spectra of K-type stars, to the cool secondary star AH Her B. Another

Table 2. Orbit parameters for AH Her.

Emission Wings		1980 Hβ	1981 Hα	Adopted
K	$(km\ s^{-1})$	124±5	134±9	126±4
γ	$(km\ s^{-1})$	−19±4	−16±4	
ϕ_0		0.49±0.01	0.48±0.02	
Absorption		**1980**	**1981**	**Adopted**
K	$(km\ s^{-1})$	148±10	175±13	158±8
γ	$(km\ s^{-1})$	34±9	7±9	
ϕ_0		−0.01±0.02	−0.05±0.02	

absorption feature (not shown in the Plate) is found near λ5207 in the Hβ spectra. We measured the velocities of these two features by fitting Gaussian profiles (FWHM=80 km s^{-1}) to the phase-binned spectra. In several phase bins the lines were only marginally detected. Fits of a circular orbit to these velocities yielded a preliminary estimate $K_{abs}=162\pm18$ km s^{-1}.

To compensate for the orbital motion of AH Her B, we computed 'phased' spectra by rebinning each individual spectrum to a wavelength scale shifted to remove the orbit velocity, and then summing the rebinned spectra. This technique, developed by Young & Schneider (1979), removes the velocity-smearing that otherwise would be introduced into the average spectrum, and thus greatly improves the visibility of weak lines. The phased spectra are shown in Figs 4 and 5. In each figure the uppermost spectrum is phased to remove the orbital motion of the white dwarf. The middle spectra are phased to remove the motion of the companion star, using the preliminary value of K_{abs} determined above. In addition to sharpening up the λλ6495 and 5207 features, the phased spectra reveal the presence of numerous additional weak absorption features. The bottom spectrum in each figure is a spectrum of 61 Cyg A (spectral type K5 V) for comparison.

To make use of the information present in these numerous weak absorption lines, we measured velocities with a cross-correlation technique similar to that of Stover *et al.* (1980). We first rebinned the spectra to a logarithmic wavelength scale, so that the velocity difference between adjacent pixels is uniform throughout the spectrum. The rebinning entails no loss of resolution because the spectra are highly oversampled (5–6 pixels/resolution element). We then combined the rebinned spectra of AH Her in 10 phase bins, and cross-correlated the 10 phase-binned spectra against a template spectrum of 61 Cygni A. We confined these cross-correlations to the wavelength region λλ6320–6520 in the 1981 data, and to λλ4889–5250 in 1980. The region λλ5160–5190 was omitted because the Mg I b lines appear to be absent in AH Her (Section 5.2 below). We then measured the velocity of AH Her B relative to 61 Cyg A by fitting a Gaussian to a peak in each cross-correlation function.

Fig. 8 shows the radial velocity curve of AH Her B that resulted from the cross-correlation analysis. The error bars shown are derived from the Gaussian fits to the cross-correlation peaks. The fitted orbit parameters for the 1980 and 1981 data sets, both separately and in combination, are given in Table 2. Note that the absorption line fiducial phase is offset by half a cycle relative to that of the emission wings, as expected for two components of the binary system. We adopt $K_{abs}=158\pm8$ km s^{-1} for the orbit velocity amplitude of AH Her B.

The width of the cross-correlation peak provides an estimate for the rotation velocity of AH Her B. We cross-correlated the template spectrum of 61 Cygni A against the spectra of eight

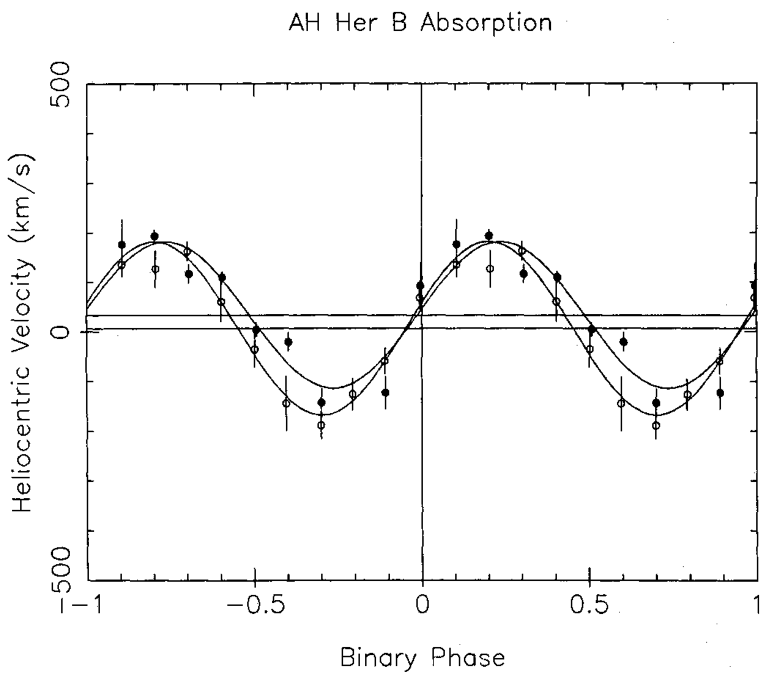

Figure 8. The velocity curve of AH Her B from cross-correlations of phase-binned spectra of AH Her with the spectrum of 61 Cyg A. Open and filled symbols denote 1980 results for the region around Hβ and 1981 results near Hα respectively. The best-fitting sine curves and horizontal lines indicating the γ velocity are also shown.

field stars of spectral type from G5 V to K7 V, and against a mean spectrum of AH Her phased to remove the orbital motion of the secondary star. The cross-correlation peaks were well fitted by Gaussian functions with dispersions for the field stars ranging from 51 to 56 km s^{-1} with a mean of $\sigma_{\rm star}=53$ km s^{-1}, and for AH Her of $\sigma_{\rm AH}=75\pm6$ km s^{-1}. We attribute the increased width of the cross-correlation peak for AH Her to the rotation of AH Her B. The dispersion of the rotational broadening profile is then given by

$$\sigma^2_{\rm rot}=\sigma^2_{\rm AH}-\sigma^2_{\rm star}. \tag{6}$$

We determined that the observed value $\sigma_{\rm rot}=53\pm8$ km s^{-1} corresponds to $V_{\rm rot}\sin i=112\pm17$ km s^{-1} by calculating the velocity dispersion for a rotating spherical star with various amounts of limb darkening.

This observed rotation velocity is in good agreement with the rotation velocity predicted by assuming that AH Her B fills its Roche-lobe and co-rotates with the binary. The predicted rotation velocity is simply

$$V_{\rm rot}\sin i=(K_W+K_R)\,\frac{R_R}{a}, \tag{7}$$

where K_W and K_R are the radial velocity semi-amplitudes of the white dwarf and red dwarf orbits, and the Roche radius R_R in units of the binary separation a is given to 1 per cent by

$$\frac{R_R}{a}=\frac{0.49\,q^{2/3}}{0.6\,q^{2/3}+\ln(1+q^{1/3})} \tag{8}$$

(Eggleton 1983) where $q=K_W/K_R$ is the mass ratio. For $K_W=K_{ems}=126\pm4\,km\,s^{-1}$ and $K_R=K_{abs}=158\pm8\,km\,s^{-1}$, the predicted velocity is $V_{rot}\sin i=102\pm3\,km\,s^{-1}$.

The orbit parameters given in Table 2 suggest that the γ velocity of the absorption lines is $37\pm10\,km\,s^{-1}$ larger than that of the emission lines. This apparent discrepancy may be an instrumental effect, since different techniques were used to measure the emission and absorption velocities. The emission lines may suffer an instrumental velocity shift because the angular distribution of the starlight that enters the spectrograph slit is slightly different from that of the light from the arc lamp. The absorption line velocities found by cross-correlating two spectra are not affected since an identical velocity shift applies to both spectra. To investigate this possibility, we measured radial velocities of several field stars by both methods. Velocities found by the cross-correlation method were systematically larger, by $+34\,km\,s^{-1}$ in 1980 and by $+20\,km\,s^{-1}$ in 1981, than velocities found by fitting a Gaussian to the Hα or Hβ absorption line in the field star spectrum. The γ velocities of emission and absorption in AH Her are not significantly different after the emission line velocities are corrected for the instrumental velocity shift. The instrumental shift of course has no affect on the measurement of K velocities.

The zero-point of our cross-correlation velocity scale was set by assuming a heliocentric radial velocity of $-65\,km\,s^{-1}$ for 61 Cygni. The velocities of the field stars we observed were reproducible to within $5\,km\,s^{-1}$ in all of our data. Our velocities agree satisfactorily with previous published radial velocities for 10 of the 11 field stars we observed in 1981, but discrepancies for two of the four stars observed in 1980 diminish our confidence in γ velocities from the 1980 data set. All velocities given in this paper are heliocentric.

5.2 THE SPECTRUM OF AH Her B

The principal absorption features visible in the phased spectrum are Fe I lines. Loose constraints were placed on the spectral type of AH Her B by considering several features whose strengths relative to Fe I vary with spectral type . Spectra of MK standard stars observed with the same instrument and mostly on the same nights as the AH Her observations were used for comparison. The absence of a sharp Hα absorption component indicates a spectral type later than K0 for AH Her B. The absence of a TiO bandhead at λ4955 requires AH Her B to be earlier than type M0, and the absence of the MgH λ4780 band requires it to be earlier than K5. On this basis AH Her B appears to be an early K dwarf.

We find that the equivalent widths of the $\lambda\lambda$6495 and 5207 features in cool dwarf stars are independent of spectral type to better than 20 per cent for spectral types G5 V to K7 V. The equivalent widths are reduced in the AH Her spectra by the additional continuum from the accretion disc. If the strengths of these features from the photosphere of AH Her B are the same as their strengths in normal K-type dwarfs, their diminished equivalent widths in the phased spectra indicate that AH Her B contributes 30–40 per cent of the total light from the system at λ6500 and only 10–15 per cent of the light at λ5200. In combination with visual magnitudes provided by the AAVSO (Table 1) and the spectral energy distribution of AH Her (Wade 1982), these estimates of the fraction of light due to AH Her B indicate that its visual magnitude is $V=15.4\pm0.3$, and suggest a spectral type between K5 and M0.

The Mg I b lines ($\lambda\lambda$5167–5183) appear to be abnormally weak relative to the Fe I lines in the phased spectrum of AH Her, compared with their relative strengths in K dwarfs. The Mg I b lines are easily detected and appear at normal strength relative to Fe I in our spectrum of the bright cataclysmic variable star AE Aqr. It is possible that these lines are filled in by emission from a chromospheric region on AH Her B, perhaps heated by radiation from the accretion disc. However, we find no phase-dependent variations in trailed-spectrogram displays of this part of the spectrum.

5.3 REVISED SPECTROSCOPIC EPHEMERIS

All phases in our paper are given with respect to the ephemeris of equation 2. This preliminary ephemeris was derived from radial velocities measured by fitting Gaussians to the Balmer emission lines in the individual spectra of AH Her. In our subsequent analysis, we combined those individual spectra into 10 phase bins, in order to increase the signal-to-noise ratio, and measured radial velocities for the emission line wings and for the absorption lines of AH Her B. These velocities favour a slightly different ephemeris.

$$\begin{aligned} HJD = 2\,444\,393.696 &+ 0.258116\,E \\ \pm 0.003 &\pm 0.000004 \end{aligned} \tag{9}$$

6 Dynamical models for the AH Her binary system

To construct a dynamical model for the AH Her binary, the emission and absorption line radial velocities are interpreted as measurements of the orbital motions of the white dwarf and red dwarf component stars. The component star masses depend sensitively on the measured orbital velocities. We therefore preface our discussion of the dynamics of AH Her with some cautionary remarks concerning systematic effects that may influence the velocities.

Velocities in the accretion flow surrounding the white dwarf are large in comparison with the orbit velocity K_{ems} we have measured. A highly symmetric emission distribution and velocity field are required if K_{ems} is to approximate the semi-amplitude K_W of the white dwarf's orbital motion, which is the quantity needed for the dynamical study. We have used the wings of the emission profile to measure the orbital motion with the expectation that the wings are formed in an accretion disc region close to the white dwarf where we hope that the severe symmetry requirements will be met. However, emission line radial velocity curves for several cataclysmic variable systems have shown anomalous phase shifts amounting to as much as 32° relative to true conjunction, which can be measured from eclipse timings or from the velocity curve of the secondary star (Stover 1981 summarizes phase shift data for five dwarf novae; see also Young, Schneider & Shectman 1981). Such phase shifts indicate directly that the emission lines in some cataclysmic variables are not following the white dwarf, even in the wings.

For AH Her we find that the relationship between the emission wing and absorption line velocities is as expected for two components of a binary system – they are anti-phased and have identical γ velocities to within the uncertainties of the observations. Thus there is no direct indication that the radial velocity measurements of AH Her fail to represent the orbital motion of its component stars.

The absorption line velocities can also deviate systematically from the centre-of-mass motion of the companion star, for example if the absorption line strength is not uniformly distributed over its surface. A dramatic example of this effect is given by Hessman *et al.* (1984), who observed an increase in the absorption K velocity of SS Cyg from 155 km s^{-1} during quiescence to 200 km s^{-1} during outburst. Increased radiation from the outbursting accretion disc heats one face of the companion star and consequently shifts the absorption line region to the hemisphere facing away from the disc. As this region is farther from the centre-of-mass of the binary, K_{abs} increases during outburst.

Our measurements of AH Her were made during quiescent periods when such heating effects are at a minimum. We note also that the confinement of absorption lines to one hemisphere of the rotating star must decrease the velocity width of the absorption line by an amount comparable to the increase in K. The agreement we found in Section 5.1 between the observed and predicted rotation velocity of AH Her B therefore provides a consistency check indicating that such heating effects increase K_{abs} by less than 20 km s^{-1}.

We turn now to the dynamics of the AH Her binary, adopting $K_W = K_{ems} = 126 \pm 4\ \mathrm{km\,s^{-1}}$ and $K_R = K_{abs} = 158 \pm 8\ \mathrm{km\,s^{-1}}$. The period and K velocities imply

$$M_W \sin^3 i = \frac{P K_R (K_W + K_R)^2}{2\pi G} = 0.34 \pm 0.04\, M_\odot, \tag{10}$$

$$M_R \sin^3 i = \frac{P K_W (K_W + K_R)^2}{2\pi G} = 0.27 \pm 0.03\, M_\odot, \tag{11}$$

and

$$a \sin i = \frac{P (K_W + K_R)}{2\pi} = 1.45 \pm 0.05\, R_\odot. \tag{12}$$

A solution for the component masses is possible if the inclination is known. The absence of photometric eclipses requires $i \lesssim 70°$. This is the condition that the centre of the accretion disc is never screened from view by the secondary star. An inclination smaller than about 37° results in a mass for the accreting star in excess of the Chandrasekhar limit $M_{chandra} = 1.44\, M_\odot$.

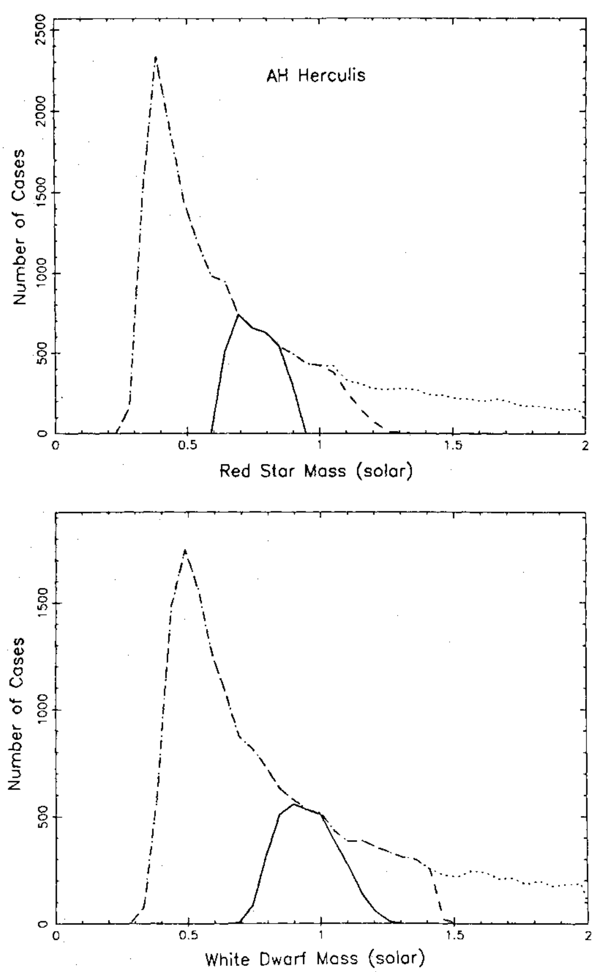

Figure 9. The posterior probability density functions for the masses of the white dwarf and red dwarf components of AH Her. Three distributions are given. The broadest of these allows the full range of inclinations consistent with the absence of eclipses (dotted line). If the white dwarf mass is required to be less massive than $1.44\, M_\odot$, the high-mass tails of the distributions are eliminated (dashed line). If an empirical main sequence mass–radius relationship is imposed on the secondary star, the narrowest distributions result (solid line).

Because the observations permit solutions over a broad range of inclination, we use a Monte Carlo technique to compute posterior probability density functions for the masses of the two component stars in AH Her. We assume that the binary period is precisely known, and employ a random number generator to sample K_R, K_W, and i, assuming Gaussian distributions (using our measured values to define the mean and standard deviation) for the two K velocities, and a uniform distribution for $0° < i < 90°$. Component masses are then calculated for a large number of samples and accumulated in mass bins to build up a histogram. High-inclination solutions that would require an eclipse of the white dwarf by the companion star are discarded.

The broadest of three mass distributions shown in Fig. 9 results from the above prescription. The use of a distribution uniform in $\cos i$ or $\sin i$ rather than in i changes the detailed shape of the broad envelope, but does not appreciably alter the range of allowed masses. If solutions with white dwarf masses larger than $1.44\,M_\odot$ are rejected in the Monte Carlo simulation, the high-mass tails are removed from the mass distributions. The narrowest of three mass distributions results from the additional requirement that the secondary star, assumed to fill its critical Roche volume, lie on an empirical main-sequence mass-radius relation:

$$\log_{10}\frac{R}{R_\odot} = 0.917\log_{10}\frac{M}{M_\odot} - 0.02 \tag{13}$$

(Lacy 1977). We implemented this last constraint by rejecting solutions that made the Roche volume-equivalent radius (equation 8) deviate more than 10 per cent from Lacy's relation. This range is allowed by the uncertainties in the mass and radius determinations of the eclipsing binaries CM Dra and YY Gem, upon which the Lacy relation primarily depends.

The posterior probability distributions are an honest way of representing the uncertainty with which the component masses can be determined given the uncertainties in our determinations of the K velocities of the two stars. Systematic errors, such as those mentioned at the beginning of this section, are not included. The considerable uncertainty in the component masses is due primarily to our present ignorance of the inclination, unless one is willing to impose a mass–radius relation on the secondary star. A measurement in the infrared of the ellipsoidal variations of AH Her B would help determine the inclination (e.g. Berriman *et al.* 1983).

If we do assume that AH Her B lies on the empirical ZAMS, then the inclination is confined to $i = 46° \pm 3°$, the component star masses are $M_W = 0.95 \pm 0.10\,M_\odot$ and $M_R = 0.76 \pm 0.08\,M_\odot$. and the binary separation is $2.04 \pm 0.07\,R_\odot$. The uncertainties, derived from the Monte Carlo simulation, stem about equally from statistical uncertainties in the K velocities and from the assumed width of the empirical mass–radius relationship.

We also computed the inner and outer limits of the Balmer emission line region from the relation

$$\frac{R}{a} = \frac{(K_W + K_R)K_R}{V^2}, \tag{14}$$

which assumes a Keplerian velocity field in the accretion disc. The observed peak-to-peak separation, $2V = 600 \pm 80\ \mathrm{km\,s^{-1}}$, implies that the outer disc radius occurs at $R_D/a = 0.50 \pm 0.14$. The emission detected at $V = 1300\ \mathrm{km\,s^{-1}}$ in the wings of Hα (Fig. 3) arises from a region 18 times smaller in radius. For comparison, the distance between the white dwarf and the inner Lagrangian point is $R_{L1}/a = 0.53$, and the mean radius of the white dwarf Roche lobe is $R_1/a = 0.40$. The accretion disc thus appears to be too large to fit comfortably within its Roche lobe. A similar anomaly has been noted for the nova-like variable RW Tri (Kaitchuck, Honeycutt & Schlegel 1983). This inconsistency may signal that our measured K velocities are too large, or

Table 3. Dynamical parameters for AH Her.

HJD_0	2444393.696 ± 0.003	
P	$0.258116 \pm 0.000004 d$	
K_W	126 ± 4 $km\ s^{-1}$	
K_R	158 ± 8 $km\ s^{-1}$	
$V_{rot} \sin i$	112 ± 17 $km\ s^{-1}$	
V_D	300 ± 40 $km\ s^{-1}$	
$M_W \sin^3 i$	0.34 ± 0.04 $M_\odot$	
$M_R \sin^3 i$	0.27 ± 0.03 $M_\odot$	
$q = M_R/M_W$	0.80 ± 0.05	
$a \sin i$	1.45 ± 0.05 $R_\odot$	
R_D/a	0.50 ± 0.13	(2)
i	$46° \pm 3°$	(1,3)
M_W	0.95 ± 0.10 $M_\odot$	(1,3)
M_R	0.76 ± 0.08 $M_\odot$	(1,3)
a	2.04 ± 0.07 $R_\odot$	(1,3)
R_W	0.008 ± 0.001 $R_\odot$	(1,3)
R_R	0.74 ± 0.03 $R_\odot$	(1,3)
R_D	1.01 ± 0.25 $R_\odot$	(1,2,3)

Assumptions: (1) Roche geometry, (2) Keplerian disc velocities,

(3) Lacy(1977) empirical main-sequence mass-radius relationship

that the measured peak-to-peak separation is too small, or perhaps both. Until this problem is resolved, stellar masses derived from the *K*-velocities must be regarded with some concern.

Our spectroscopic observations have allowed us to determine the binary period and the radial velocity semi-amplitudes of both components of the AH Her binary. On the basis of these measurements we have examined a dynamical model of the system. The model is summarized in Table 3, which collects our estimates of the parameters of the AH Her binary and indicates the assumptions upon which they rest.

Acknowledgments

We thank the Director of Mt Wilson Observatory for the generous allocation of observing time. Analysis of the data was carried out at the California Institute of Technology and on the Cambridge node of the SERC STARLINK network. KDH thanks the SERC for financial support.

References

Berriman, G., Beattie, D. H., Gatley, I., Lee, T. J., Mochnacki, S. W. & Szkody, P., 1983. *Mon. Not. R. astr. Soc.*, **204**, 1105.

Bretz, M., 1965. Position of variable stars in the Hertzsprung-Russell diagram, *Kleinere Veröff. Bamberg IV*, No. 40, 244.

Echevarria, J., 1983. *DPhil thesis*, University of Sussex.

Echevarria, J. & Jones, D. H. P., 1984. *Mon. Not. R. astr. Soc.*, **206**, 919.

Eggleton, P. P., 1983. *Astrophys. J.*, **268**, 368.

Hessman, F. V., Robinson, E. L., Nather, R. E. & Zhang, E.-H., 1984. *Astrophys. J.*, **286**, 747.

Hildebrand, R. H., Spillar, E. J., Middleditch, J., Patterson, J. & Stiening, R. F., 1980. *Astrophys. J.*, **238**, L145.

Hildebrand, R. H., Spillar, E. J. & Stiening, R. F., 1981. *Astrophys. J.*, **248**, 268.

Kaitchuck, R. H., Honeycutt, R. K. & Schlegel, E. M., 1983. *Astrophys. J.*, **267**, 239.
Lacy, C. H., 1977. *Astrophys. J. Suppl.*, **34**, 479.
Moffatt, A. F. J. & Shara, M. M., 1984. *Publs astr. Soc. Pacif.*, **96**, 552.
Oke, J. B. & Wade, R. A., 1982. *Astr. J.*, **87**, 670.
Patterson, J., 1981. *Astrophys. J. Suppl.*, **45**, 517.
Robinson, E. L., 1973. *Astrophys. J.*, **181**, 531.
Schneider, D. P. & Young, P., 1980. *Astrophys. J.*, **238**, 955.
Shafter, A. W., 1983. *Astrophys. J.*, **267**, 222.
Smak, J., 1969. *Acta Astron.*, **19**, 155.
Stover, R. J., 1981. *Astrophys. J.*, **249**, 673.
Stover, R. J., Robinson, E. L., Nather, R. E. & Montemayor, T. J., 1980. *Astrophys. J.*, **240**, 597.
Szkody, P. & Mattei, J. A., 1984. *Publs astr. Soc. Pacif.*, **96**, 988.
Wade, R. A., 1982. *Astr. J.*, **87**, 1558.
Wargau, W., Rahe, J. & Vogt, N., 1983. *Astr. Astrophys.*, **117**, 283.
Young, P. & Schneider, D. P., 1979. *Astrophys. J.*, **230**, 502.
Young, P., Schneider, D. P. & Shectman, S. A., 1981. *Astrophys. J.*, **244**, 259.